DINAME 2017 - Proceedings of the XVII International Symposium on Dynamic Problems of Mechanics
A. T. Fleury, D. A. Rade, P. R. G. Kurka (Editors), ABCM, São Sebastião, SP, Brazil, March 5-10, 2017

INFLUENCE OF VISCOELASTIC DAMPING ON THE DYNAMIC RESPONSE OF NONLINEAR AEROELASTIC SYSTEMS

Thiago de P. Sales[a], Daniel A. Pereira[b], Flávio D. Marques[c] and Domingos A. Rade[b]

[a] School of Mechanical Engineering, Federal University of Uberlândia, Uberlândia, MG, Brazil
[b] Mechanical Engineering, Aeronautics Institute of Technology, São José dos Campos, SP, Brazil
[c] Engineering School of São Carlos, University of São Paulo, Brazil

Abstract: Nonlinear aeroelastic systems are prone to the appearance of limit cycle oscillations, bifurcation and chaos. Such problems are of increasing concern in aircraft design since there is the need to control nonlinear instabilities and improve safety margins, at the same time as aircraft are subjected to increasingly critical operational conditions. On the other hand, viscoelastic materials have already been successfully used for the attenuation of undesired vibrations in several types of mechanical systems. However, a considerably small number of research works have addressed the feasibility of exploring the viscoelastic effect to improve the behavior of nonlinear aeroelastic systems. In this context, the objective of this work is to assess the influence of viscoelastic materials on the aeroelastic features of three-degree-of-freedom typical section models (including pitch, plunge and control surface motions) which present structural nonlinearities of the hardening stiffness type. The equations of motion of the system under analysis are derived in such a way that one is able to account for the dependence of the viscoelastic material properties on frequency and temperature. For this purpose, a constitutive law based on fractional derivatives is adopted, allowing for the modeling of the viscoelastic behavior in the time domain. The aerodynamic forces are introduced based on the classical theory of linear unsteady aerodynamics with corrections for arbitrary motions derived from Theodorsen's method. The aeroelastic behavior is investigated through time domain simulations, and subsequent frequency transforms, from which bifurcations are identified, and diagrams of vibration amplitudes versus airspeed are constructed to characterize the conditions under which the system is supercritical or subcritical. The influence of the viscoelastic effect on the aeroelastic behavior, for different values of temperature, is highlighted and discussed. Numerical simulation shows that viscoelastic damping can increase noticeably the flutter speed and reduce the amplitudes of limit cycle oscillations for the system under consideration. These results show that viscoelastic materials can be used in the aircraft components to increase safety margins of the flight envelope as related to the aeroelastic stability. The authors acknowledge the CNPq, FAPEMIG, and FAPESP for their continuing financial support of research activities.

Keywords: nonlinear aeroelasticity, typical section model, cubic hardening, viscoelasticity, damping, flutter, limit cycle oscillation

INTRODUCTION

The aeroelasticity is a multidisciplinary field of study that belongs to the aerospace engineering, which deals with the interaction between structural dynamics and non-stationary aerodynamic flow. This multidisciplinary nature is better explained through Collar's Triangle (Collar, 1946). This triangle represents the interactions between three disciplines: aerodynamics, dynamics, and elasticity. Classical aerodynamic theories provide a prediction of the forces acting on a body of a given shape. Elasticity provides a prediction of the shape of an elastic body under a given load. Dynamics introduces the effects of inertial forces (Hodges and Pierce, 2011).

Aeroelastic systems may present nonlinearities, therefore subject to undesirable behaviors such as bifurcations, limit cycle oscillations (LCOs), and chaos (Sheta *et al.*, 2002). It is known that nonlinear behaviors, whose origins are both from structural dynamics or from the unsteady aerodynamic loading, are difficult to predict and are associated with destructive structural responses (Dowell *et al.*, 2003). For example, LCOs have caused persistent problems in many aircraft designs, such as the F-16 (Chen *et al.*, 1998). In general, linear models used in designs are conservative due to the requirement of safety margins to ensure stability to the aircraft even under the influence of nonlinear effects (Henshaw et al., 2007).

Among the sources of nonlinearities in aeroelastic systems, the structural nonlinearities have been extensively studied by many authors during the last years. Concentrated nonlinear effects, the most well-known example of structural nonlinearities, can be incorporated into numerical models through elastic restoring forces or moments representations. The traditional and well-understood types of concentrated nonlinearities are the hardening and softening springs, which can be approximated by polynomial functions (O'Neil and Strganac, 1998), free-play (Vasconcellos *et al.*, 2012) and hysteresis (Chung *et al.*, 2009). On the other hand, not much is known about the fundamental mechanisms of damping and their impact on flutter and LCOs (Dowell *et al.*, 2014). The internal damping forces may also have a nonlinear relationship to the structural motion expressing a great challenge to the engineers, consequently, they are usually represented empirically even in linear aeroelastic mathematical models.

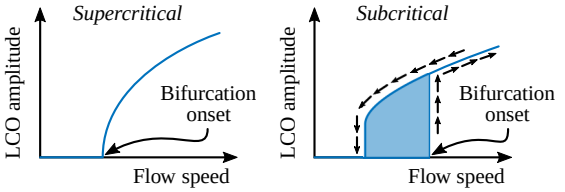

Figure 1 – Supercritical and subcritical Hopf bifurcations. The shaded region exhibits unstable behavior.

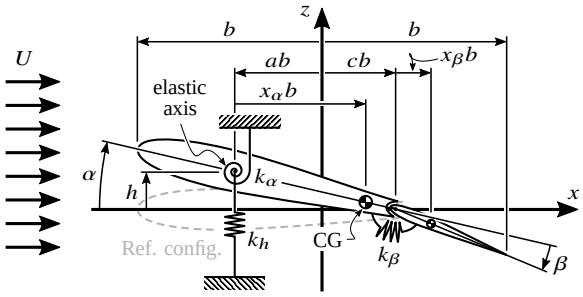

Figure 2 – Physical model for the 3 DOFs typical section aeroelastic system.

A generic way to analyze the nonlinear system behavior is by bifurcation diagram, where the limit cycle amplitude is plotted versus some system parameter, such as the flight speed. Bifurcation analysis is used to indicate a quantitative and qualitative change in the features of a system, such as the number and type of solutions, under the variation of one or more parameters on which the considered system depends (Nayfeh and Balachandran, 2008). Figure 1 depicts classical bifurcation diagrams for supercritical and subcritical behaviors. In general, if the system depends on the initial conditions and has different solutions when the airspeed velocity is increased and decreased near the nonlinear critical velocity, the bifurcation is called subcritical, i.e. LCO may also exist below the flutter boundary (unstable LCO, shaded region). However, if the system is independent of the initial conditions and its stability changes only after the critical flutter velocity, the bifurcation is called supercritical.

During the design of an aeroelastic system, it might be a requirement to further improve stability margins and reduce LCO amplitudes related to flutter conditions. Usually this is the case, as aeroelastic phenomena is overlooked during preliminary design phases, and only accounted for in later stages when prototype manufacture has already began. To remedy the situation, structural modifications can be useful, and, in this work, one proposes the use of viscoelastic damping for that matter.

Viscoelastic materials have already been proven as a viable solution for several vibration-related engineering problems (Rao, 2003). This class of materials combines the behavior of elastic solids and Newtonian fluids, in the sense that such materials not only store, but also dissipate energy, in a passive manner. However, their application requires carefulness, since material properties are dependent on several environmental and operating conditions. These encompass, among others, temperature, frequency, and static pre-load (Nashift *et al.*, 1985). Modeling of viscoelastic behavior must be done accordingly, and several strategies have been put forward to allow design and prediction of complex engineering systems that contain viscoelastic damping (Lakes, 2009).

Viscoelastic damping has already been adopted for flutter control. Lacarbonara and Cetraro (2011) proposed a visco-hysteretic vibration absorber (VA) to increase the flutter speed and to improve the damping in the pre- and post-flutter regimes of a one-degree-of-freedom typical section. Martins *et al.* (2017) performed experimental and numerical analysis of two-degree-of-freedom typical section presenting viscoelastic material in pitch and plunge motion, they have shown that the viscoelastic material can increase considerably the flutter speed. Some other authors have reported the viscoelastic damping treatments to avoid panel flutter in supersonic regime (Cunha *et al.*, 2016). Despite their contributions, these studies have been limited to cases of linear aeroelastic systems.

Thus, in this work, one investigates the influence of viscoelastic damping in a nonlinear aeroelastic system, which consists of a typical section with plunge, pitch and control surface degrees of freedom, with cubic-hardening nonlinear behavior for the pitch angle stiffness. As one deals with a nonlinear system, traditional flutter analysis methods do not prove adequate, and numerical time integration is performed. For this reason, to model viscoelastic behavior, a fractional differential equation is adopted for the constitutive relation. As to unsteady aerodynamic loads, the classical theory with corrections for arbitrary motion is employed.

In the following Section, physical modeling is addressed. Later on, numerical results and conclusions are given.

PHYSICAL MODELS

Three DOF Nonlinear Aeroelastic Typical Section System

The mathematical model for a typical section, as shown in Figure 2, is derived admitting the basic principles given in Bisphinghoff *et al.* (1996) and Theodorsen (1935). Accounting for nonlinear stiffness behavior in the pitch and control surface degrees of freedom, one can write:

$$\begin{bmatrix} \mu_e & x_\alpha & x_\beta \\ x_\alpha & r_\alpha^2 & [r_\beta^2+(c-a)x_\beta] \\ x_\beta & [r_\beta^2+(c-a)x_\beta] & r_\beta^2 \end{bmatrix} \begin{Bmatrix} \ddot{\xi}(t) \\ \ddot{\alpha}(t) \\ \ddot{\beta}(t) \end{Bmatrix} + \begin{bmatrix} d_{1,1} & d_{1,2} & d_{1,3} \\ d_{2,1} & d_{2,2} & d_{2,3} \\ d_{3,1} & d_{3,2} & d_{3,3} \end{bmatrix} \begin{Bmatrix} \dot{\xi}(t) \\ \dot{\alpha}(t) \\ \dot{\beta}(t) \end{Bmatrix} + \begin{bmatrix} \omega_h^2 & 0 & 0 \\ 0 & r_\alpha^2\omega_\alpha^2 \frac{F(\alpha)}{\alpha(t)} & 0 \\ 0 & 0 & r_\beta^2\omega_\beta^2 \frac{F(\beta)}{\beta(t)} \end{bmatrix} \begin{Bmatrix} \xi(t) \\ \alpha(t) \\ \beta(t) \end{Bmatrix} = \begin{Bmatrix} -L(t)/(m_W b) \\ M_\alpha(t)/(m_W b^2) \\ M_\beta(t)/(m_W b^2) \end{Bmatrix}, \quad (1)$$

where t denotes time; the plunge, pitch and control surface displacements are given by h, α, and β, respectively; a and c are the dimensionless distances from the elastic axis to the middle and to the surface control; U is the airspeed; x_α and x_β are the dimensionless distances from the elastic axis to the wing center of gravity (CG) and the distance between the control surface and its CG, respectively; k_h, k_α, and k_β are the plunge, pitch and control surface stiffness, respectively; $\xi = h/b$; $\mu_e = m_T/m_W$; $d_{i,j}$ are the damping factors with respect to each airfoil motion and their influences; $L(t)$ is the lift force; $M_\alpha(t)$ and $M_\beta(t)$ are the aerodynamic pitch and hinge moments, respectively; and $F(\alpha)$ and $F(\beta)$ are functions related to nonlinearities in α and β stiffness. As to notation, $\dot\bullet = \mathrm{d}\bullet/\mathrm{d}t$, and $\ddot\bullet = \mathrm{d}^2\bullet/\mathrm{d}t^2$.

Aerodynamic modeling is based on the formulation by Theodorsen (1935), who presents an analytical solution to the pressure distribution around a typical airfoil section using 2-D irrotational, incompressible and potential flow assumptions, which are subject to harmonic motions. The convolution of Wagner function is used to expand the Theodorsen function in order to account for arbitrary airfoil motions. Details on this approach can be obtained from Vasconcellos *et al.* (2016).

Given the previous arguments, the equations of motion for the aeroelastic system can be presented in the following final form:

$$(\mathbf{M}_s - \mathbf{M}_{nc})\ddot{\mathbf{x}} + (\mathbf{C}_s - \mathbf{C}_{nc} - \tfrac{1}{2}\mathbf{R}\mathbf{S}_2)\dot{\mathbf{x}} + (\mathbf{K}_s - \mathbf{K}_{nc} - \tfrac{1}{2}\mathbf{R}\mathbf{S}_1)\mathbf{x} - \mathbf{R}\mathbf{S}_3\mathbf{x}_a = \mathbf{0}; \tag{2}$$

$$\dot{\mathbf{x}}_a - \mathbf{E}_1\mathbf{x} - \mathbf{E}_2\dot{\mathbf{x}} - \mathbf{F}\mathbf{x}_a = \mathbf{0}, \tag{3}$$

where $\mathbf{x} = [\ \xi \quad \alpha \quad \beta\ ]^{\mathrm{T}}$ is the vector of structural generalized degrees of freedom, and $\mathbf{x}_a = [\ x_a \quad \dot{x}_a\ ]^{\mathrm{T}}$ is the vector of augmented aerodynamic states. Expressions for the matrices appearing in Eqs. (2) – (3) can be found in Vasconcellos *et al.* (2016). $\mathbf{M}_s$, $\mathbf{C}_s$, and $\mathbf{K}_s$ are the structural mass, damping and stiffness matrices, respectively; $\mathbf{M}_{nc}$, $\mathbf{C}_{nc}$, and $\mathbf{K}_{nc}$ are the non-circulatory flow contributions to mass, damping and stiffness matrices of the system, respectively; and $\mathbf{R}$, $\mathbf{S}_1$, $\mathbf{S}_2$, $\mathbf{S}_3$, $\mathbf{E}_1$, $\mathbf{E}_2$, and $\mathbf{F}$ are matrices and vectors that arise from the circulatory flow formulation, and that modify damping and stiffness properties, and couple the structural response with the time evolution of the augmented aerodynamic states.

Fractional Derivative Viscoelastic Constitutive Behavior

The model used for the constitutive behavior of a viscoelastic damper is now considered. It makes use of the so-called fractional derivatives, and generalizes on the standard linear solid for a better representation of the frequency-dependency of the complex moduli of a viscoelastic material. Temperature-dependency can also be accounted for, as will be shown.

The constitutive relationship is such that (Galucio *et al.*, 2004):

$$\sigma_v + \tau_v^{\alpha_v}\frac{\mathrm{d}^{\alpha_v}}{\mathrm{d}t^{\alpha_v}}\sigma_v = E_{0v}\epsilon_v + E_{\infty v}\tau_v^{\alpha_v}\frac{\mathrm{d}^{\alpha_v}}{\mathrm{d}t^{\alpha_v}}\epsilon_v, \tag{4}$$

where σ_v is the stress; ϵ_v is the strain; and τ_v, E_{0v}, $E_{\infty v}$, α_v are the model parameters. Physically, τ_v is a relaxation time constant, whereas E_{0v} and $E_{\infty v}$ are the viscoelastic stiffness moduli for low and high frequencies, respectively. Moreover, $\mathrm{d}^{\alpha_v}/\mathrm{d}t^{\alpha_v}$ denotes fractional differentiation of order $\alpha_v \in \mathbb{R}_+^*$, according to Caputo's definition (Galucio *et al.*, 2004; Diethelm, 2010). It should be noted that, due to constraints that arise from the 2nd Law of Thermodynamics, the following conditions must be met (Bagley and Torvik, 1986):

$$E_{0v} \geq 0, \qquad E_{\infty v} > 0, \qquad \tau_v^{\alpha_v} > 0, \qquad E_{\infty v} \geq E_{0v}. \tag{5}$$

The model also presumes that $0 < \alpha_v < 1$.

To adopt Eq. (4) as the constitutive equation for viscoelastic behavior, and use it within a structural modeling scheme, a good strategy consists of expressing σ_v explicitly. For this, one employs the Grünwald-Letnikov approximation of a fractional derivative (Galucio *et al.*, 2004):

$$\frac{\mathrm{d}^{\alpha_v}}{\mathrm{d}t^{\alpha_v}} f(t) \cong (\Delta t)^{-\alpha_v} \sum_{k=0}^{N_v} \Big[g_{k+1}\, f(t - k\Delta t) \Big], \tag{6}$$

where N_v is the number of terms used in the approximation, and g_{k+1} are the so-called Grünwald coefficients. These may be computed according to $g_{k+1} = [(k - 1 - \alpha_v)/k]\ g_k$ for $k = 1, \ldots, N_v$, with $g_1 := 1$.

Equation (4) can be rewritten by considering the internal variable $\overline{\epsilon}_v = \epsilon_v - \sigma_v/E_{\infty v}$. This leads to:

$$\overline{\epsilon}_v + \tau_v^{\alpha_v}\frac{\mathrm{d}^{\alpha_v}}{\mathrm{d}t^{\alpha_v}}\overline{\epsilon}_v = \left(\frac{E_{\infty v} - E_{0v}}{E_{\infty v}}\right)\epsilon_v, \tag{7}$$

which is useful since only one fractional derivative will be discretized with the help of Eq. (6).

By using Eq. (6) for the fractional derivative of $\overline{\epsilon}_v$, after algebraic manipulations it is possible to write:

$$\overline{\epsilon}_v = \left[\frac{(\Delta t)^{\alpha_v}}{(\Delta t)^{\alpha_v} + \tau_v^{\alpha_v}}\right]\left(\frac{E_{\infty v} - E_{0v}}{E_{\infty v}}\right)\epsilon_v - \frac{\tau_v^{\alpha_v}}{(\Delta t)^{\alpha_v} + \tau_v^{\alpha_v}} \sum_{k=1}^{N_v} \Big[g_{k+1}\overline{\epsilon}_v(t - k\Delta t) \Big], \tag{8}$$

where it is to be understood that $\epsilon_v \equiv \epsilon_v(t)$, and $\overline{\epsilon}_v \equiv \overline{\epsilon}_v(t)$. In the adopted notation, t now denotes a discrete time instant. Considering the definition adopted for $\overline{\epsilon}_v$, σ_v can be expressed as:

$$\sigma_v = E_{0v}\left\{ \left[1 + c_v \left(\frac{E_{\infty v} - E_{0v}}{E_{0v}}\right)\right]\epsilon_v + c_v\frac{E_{\infty v}}{E_{0v}} \sum_{k=1}^{N_v} \Big[g_{k+1}\overline{\epsilon}_v(t - k\Delta t) \Big] \right\}, \tag{9}$$

where $c_v = \tau_v^{\alpha_v}\left[(\Delta t)^{\alpha_v} + \tau_v^{\alpha_v}\right]^{-1}$. Given σ_v, a viscoelastic damper can be incorporated to an existing structural model by considering the generalized forces it produces, through the use of the virtual work principle, for example.

Parameter Identification and Temperature Dependence

The identification of the 4 parameters E_{0v}, $E_{\infty v}$, τ_v, and α_v for a given viscoelastic material can be performed in the frequency domain. Accounting for properties of fractional derivatives, the Fourier transform of Eq. (4) leads to:

$$E(\mathrm{j}\omega) = \sigma(\mathrm{j}\omega)/\epsilon(\mathrm{j}\omega) = \frac{E_{0v}+E_{\infty v}(\tau_v \mathrm{j}\omega)^{\alpha_v}}{1+(\tau_v \mathrm{j}\omega)^{\alpha_v}}, \tag{10}$$

where $\mathrm{j} = \sqrt{-1}$ is the imaginary unit, ω is the circular frequency, and $E(\mathrm{j}\omega)$ is the longitudinal complex modulus associated with the fractional derivative model.

The inverse identification problem relies on the availability of a reference data set. In this work, curves presented by Soovere and Drake (1984), fitted to gathered experimental data, are used. Soovere and Drake (1984) also account for the temperature-frequency equivalence principle in their work. It states that changes in the complex modulus due to frequency variations are equivalent to shifts along the temperature axis (Nashif *et al.*, 1985). For this reason, the concept of a reduced frequency ω_R can then be introduced, such that:

$$\omega_R = \gamma(T)\,\omega, \tag{11}$$

where $\gamma(T)$ is the shift-factor function.

Soovere and Drake (1984) present data as a set of analytical functions $G(\mathrm{j}\omega_R)$ and $\gamma(T)$. From Eq. (10), it is then desirable to write the model complex modulus as:

$$G(\mathrm{j}\omega_R) = \frac{E(\mathrm{j}\omega_R)}{2(1+\nu)} = \frac{G_{0v}+G_{\infty v}(\tau_v \mathrm{j}\omega_R)^{\alpha_v}}{1+(\tau_v \mathrm{j}\omega_R)^{\alpha_v}}, \tag{12}$$

where ν is the viscoelastic material Poisson's ratio. It is assumed that it is frequency-independent, although this is not a proper assumption for every case (Lakes, 2009).

The identification procedure can finally be solved by considering an optimization problem with the following objective function:

$$F_{\mathrm{obj}}(G_{0v}, G_{\infty v}, \tau_v, \alpha_v) = \frac{1}{n}\sum_{\omega_R=\omega_{R_1}}^{\omega_{R_n}} \left[\frac{\Re\{G_{\mathrm{model}}(\mathrm{j}\omega_R, G_{0v}, G_{\infty v}, \tau_v, \alpha_v)\} - \Re\{G_{\mathrm{ref}}(\mathrm{j}\omega_R)\}}{\Re\{G_{\mathrm{ref}}(\mathrm{j}\omega_R)\}}\right]^2 + \frac{1}{n}\sum_{\omega_R=\omega_{R_1}}^{\omega_{R_n}} \left[\frac{\Im\{G_{\mathrm{model}}(\mathrm{j}\omega_R, G_{0v}, G_{\infty v}, \tau_v, \alpha_v)\} - \Im\{G_{\mathrm{ref}}(\mathrm{j}\omega_R)\}}{\Im\{G_{\mathrm{ref}}(\mathrm{j}\omega_R)\}}\right]^2, \tag{13}$$

where $\Re$ and $\Im$ are used to denote the real and imaginary components of a given complex quantity, G_{model} is computed using Eq. (12), and G_{ref} is the reference data set.

An important remark is now made on how to incorporate temperature dependence in the model by identifying a single set of parameters in the reduced frequency space. If one substitute Eq. (11) into Eq. (12), one can group the shift factor function $\gamma(T)$ with the parameter τ_v, and then write:

$$G(\mathrm{j}\omega, T) = \frac{E(\mathrm{j}\omega, T)}{2(1+\nu)} = \frac{G_{0v}+G_{\infty v}\left[\tau_v^*(T)\mathrm{j}\omega\right]^{\alpha_v}}{1+\left[\tau_v^*(T)\mathrm{j}\omega\right]^{\alpha_v}}, \tag{14}$$

where $\tau_v^*(T) = \tau_v \gamma(T)$, and τ_v is the value of identified for the case in which $\gamma(T) = 1$, i.e. when $\omega = \omega_R$.

Three DOFs Nonlinear Aeroelastic Typical Section System With Viscoelastic Dampers

To incorporate viscoelastic dampers into the model, Eq. (2) is modified to:

$$(\mathbf{M}_s - \mathbf{M}_{nc})\ddot{\mathbf{x}} + (\mathbf{C}_s - \mathbf{C}_{nc} - \tfrac{1}{2}\mathbf{R}\mathbf{S}_2)\dot{\mathbf{x}} + (\mathbf{K}_s + \tilde{\mathbf{K}}_v - \mathbf{K}_{nc} - \tfrac{1}{2}\mathbf{R}\mathbf{S}_1)\mathbf{x} - \mathbf{R}\mathbf{S}_3\mathbf{x}_a = -c_v \frac{E_{\infty v}}{E_{0v}}\mathbf{K}_v \sum_{k=1}^{N_v}\left[g_{k+1}\overline{\mathbf{x}}(t-k\Delta t)\right], \tag{15}$$

where $\tilde{\mathbf{K}}_v = \left(1 + c_v\frac{E_{\infty v}-E_{0v}}{E_{0v}}\right)\mathbf{K}_v$, and:

$$\mathbf{K}_v = G_{0v}\begin{bmatrix} \frac{k_{hv}}{m_W} & 0 & 0 \\ 0 & \frac{k_{\alpha v}}{m_W b^2} & 0 \\ 0 & 0 & \frac{k_{\beta v}}{m_W b^2} \end{bmatrix}. \tag{16}$$

k_{hv}, $k_{\alpha v}$, and $k_{\beta v}$ are constants related to the geometric arrangement of each viscoelastic damper. Equation (16) shows G_{0v} factored out since one assumes that the viscoelastic dampers work by exploiting shear deformation modes; also, the factors $m_W b^2$ and m_W are due to the normalization of the aeroelastic equations.

To further clarify on how the dampers would work in practice, their geometry is shown in Fig. 3. Their implementation on the physical model is displayed in Fig. 4 – the formulation presented for $\mathbf{K}_v$ above corresponds to the situation in which the parallel mechanical arrangement shown in this figure is assumed. Now, considering the shear deformation for the viscoelastic layers, it is possible to show that:

$$k_{hv} = 2l_h\left(\frac{d_3}{d_2}\right)_h; \quad k_{\alpha v} = 2\pi(R_{\mathrm{mean}})_\alpha^2\,(d_3)_\alpha; \quad k_{\beta v} = 2\pi(R_{\mathrm{mean}})_\beta^2\,(d_3)_\beta, \tag{17}$$

where the subscripts h, α, and β are used to distinguish between the geometric dimensions related to the viscoelastic dampers adopted for each of the degrees of freedom.

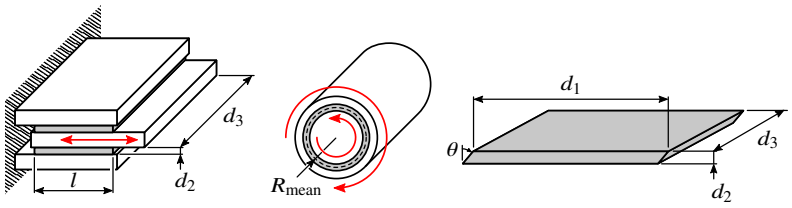

(a) Translational damper (b) Rotational damper (c) Shear deformation mechanism acting on the viscoelastic layers

Figure 3 – Geometry of the viscoelastic dampers. Viscoelastic material is shown in gray.

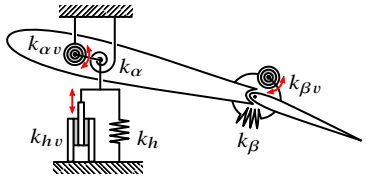

Figure 4 – Physical model for the 3 DOFs typical section with viscoelastic dampers arranged in parallel.

Numerical Solution Procedures

The procedures adopted for solution of the mathematical model presented earlier are now considered. First, it is of interest to identify the nature of the equations one deals with. Equation (15) represents a set of coupled nonlinear second-order ODEs. Equation (3), on the other hand, is a set of coupled linear first-order ODEs. Both of these sets need to be considered simultaneously during the solution procedure. Moreover, another point that deserves attention is the approach adopted for incorporation of the viscoelastic dampers, through the use of fractional derivatives. This choice implies in the need of a specialized procedure for obtaining a numerical solution.

One starts by first rewriting Eqs. (3) and (15) in the state space form:

$$\dot{\mathbf{X}} = \mathbf{A}\mathbf{X} + \mathbf{B} \tag{18}$$

where $\mathbf{X} = \begin{bmatrix} \mathbf{x}^{\mathrm{T}} & \dot{\mathbf{x}}^{\mathrm{T}} & \mathbf{x}_a^{\mathrm{T}} \end{bmatrix}^{\mathrm{T}}$ is the state vector, and:

$$\mathbf{A} = \begin{bmatrix} \mathbf{0}_{(3\times3)} & \mathbf{I}_3 & \mathbf{0}_{(3\times2)} \\ -\mathbf{M}^{-1}\mathbf{K} & -\mathbf{M}^{-1}\mathbf{C} & \mathbf{M}^{-1}\mathbf{R}\mathbf{S}_3 \\ \mathbf{E}_1 & \mathbf{E}_2 & \mathbf{F} \end{bmatrix}; \quad \mathbf{B} = \begin{bmatrix} \mathbf{0}_{(3\times1)} \\ -\mathbf{M}^{-1}\mathbf{F}_v \\ \mathbf{0}_{(2\times1)} \end{bmatrix}. \tag{19}$$

Also, the following shorthands have been used:

$$\mathbf{K} = \mathbf{K}_s + \tilde{\mathbf{K}}_v - \mathbf{K}_{nc} - \tfrac{1}{2}\mathbf{R}\mathbf{S}_1; \quad \mathbf{C} = \mathbf{C}_s - \mathbf{C}_{nc} - \tfrac{1}{2}\mathbf{R}\mathbf{S}_2; \quad \mathbf{F}_v = c_v \tfrac{E_{\infty v}}{E_{0v}} \mathbf{K}_v \sum\nolimits_{k=1}^{N_v} \left[g_{k+1} \overline{\mathbf{x}}(t - k\Delta t) \right]. \tag{20}$$

One equation that is still missing from the formulation is related to the computation of the internal variables associated with the viscoelastic constitutive law, $\overline{\mathbf{x}}$. It can be established by considering Eq. (8). After algebraic manipulations, and accounting for strain-displacement relationships, it is possible to arrive at (Galucio *et al.*, 2004):

$$\overline{\mathbf{x}} = (1 - c_v) \left(\tfrac{E_{\infty v} - E_{0v}}{E_{\infty v}} \right) \mathbf{x} - c_v \sum\nolimits_{k=1}^{N_v} \left[g_{k+1} \overline{\mathbf{x}}(t - k\Delta t) \right]. \tag{21}$$

To solve the set given by Eqs. (18) and (21), one employs the trapezoidal rule numerical integration scheme. It states that:

$$\mathcal{R}_{t+\Delta t} = \mathbf{X}_{t+\Delta t} - \mathbf{X}_t - \tfrac{\Delta t}{2} \left(\dot{\mathbf{X}}_{t+\Delta t} + \dot{\mathbf{X}}_t \right) = \mathbf{0}, \tag{22}$$

where the subscripts indicate the discrete time at which solution is to be evaluated.

Equation (22) is treated as a residual, for which $\dot{\mathbf{X}}$ is evaluated with the help of Eq. (18). As such, it is nonlinear. For this, the Newton-Raphson method is considered for its solution. First, it is assumed that the solution is known up to time t, and that an approximate solution set n is given for time $t + \Delta t$. The residual associated to a new solution set $n+1$ is linearized around the approximate solution set n by expanding it in a Taylor series. Higher order terms are neglected, and a linear system of equations is obtained for the increment in the approximate solution set:

$$\mathbf{J}^n_{t+\Delta t} \Delta\mathbf{X} = -\mathcal{R}^n_{t+\Delta t}, \tag{23}$$

from which the solution is updated according to:

$$\mathbf{X}^{n+1}_{t+\Delta t} = \mathbf{X}^n_{t+\Delta t} + \Delta\mathbf{X}. \tag{24}$$

In Eq. (23), $\mathbf{J}$ designates the Jacobian matrix:

$$\mathbf{J} = \tfrac{\partial \mathcal{R}}{\partial \mathbf{X}^{\mathrm{T}}} \quad \Leftrightarrow \quad J_{ij} = \tfrac{\partial \mathcal{R}_i}{\partial X_j}; \tag{25}$$

algebraic manipulations leads to:

$$\mathbf{J} = \mathbf{I}_8 - \tfrac{\Delta t}{2} (\mathbf{A} + d\mathbf{A}), \tag{26}$$

where:

$$dA_{ij} = \tfrac{\partial A_{ik}}{\partial X_j} X_k \; : \; d\mathbf{A} = \begin{bmatrix} \mathbf{0}_{(3\times3)} & \mathbf{0}_{(3\times3)} & \mathbf{0}_{(3\times2)} \\ -\mathbf{M}^{-1} d\mathbf{K} & \mathbf{0}_{(3\times3)} & \mathbf{0}_{(3\times2)} \\ \mathbf{0}_{(2\times3)} & \mathbf{0}_{(2\times3)} & \mathbf{0}_{(2\times2)} \end{bmatrix}, \quad d\mathbf{K} = \begin{bmatrix} 0 & 0 & 0 \\ 0 & r_\alpha^2 \omega_\alpha^2 \tfrac{\partial F_\alpha}{\partial \alpha} & 0 \\ 0 & 0 & r_\beta^2 \omega_\beta^2 \tfrac{\partial F_\beta}{\partial \beta} \end{bmatrix}. \tag{27}$$

The numerical solution procedure is summarized in the flowchart shown in Fig. 5.

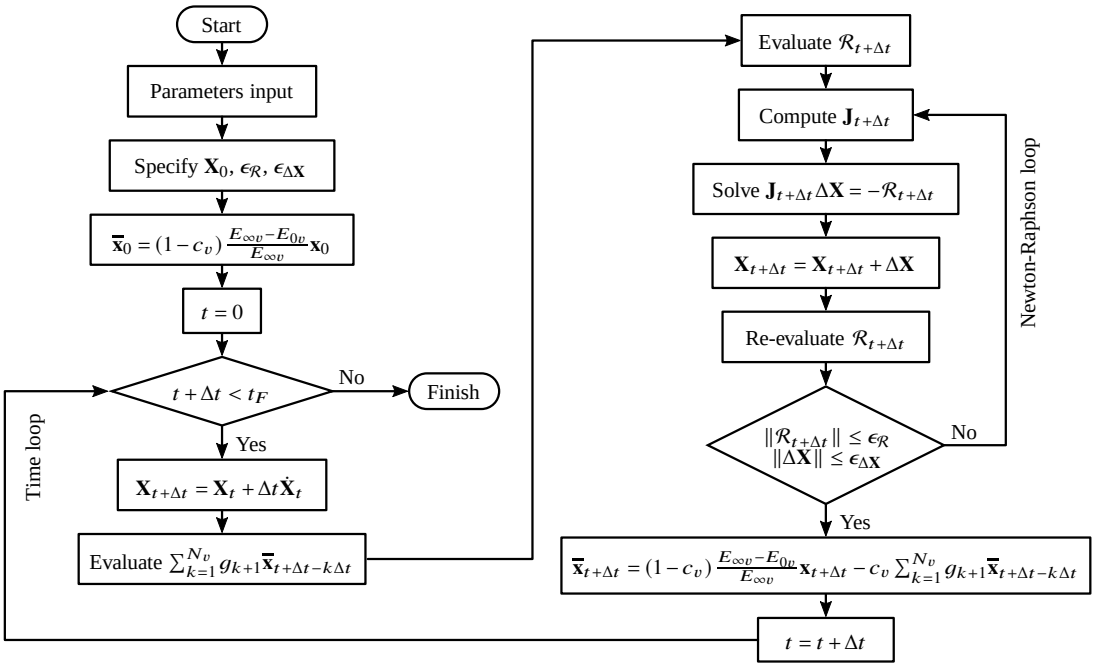

Figure 5 – Solution algorithm flowchart.

SIMULATION RESULTS AND DISCUSSIONS

The aeroelastic system model given in Eq. (18) has been numerically integrated according to the procedure described in the previous Section. Table 1 gives the system parameters and operational conditions considered for obtaining the results given in this work. One accounts for only a simple nonlinear behavior in the pitch degree of freedom. The type of the nonlinearity is of a cubic polynomial , which might be produced as in the experimental setup used by O'Neil and Strganac (1998). It has been adopted that:

$$F(\alpha) = \alpha + 3.9782\alpha^3. \tag{28}$$

This implies a hardening stiffness type for α. As for the other nonlinear stiffness function, it evaluates to $F(\beta) = \beta$. This effectively renders linear the third equation of the set shown in Eq. (1).

Time integration has been performed with a resolution of 0.005 s. Final time of simulation was set equal to 500 s, so one could be certain that steady-state regime was achieved. During preliminary simulations, it has been seen that the nonlinear behavior of the system was supercritical. Hence, the steady state response is independent of the given initial conditions, and, as such, have been adopted as $\mathbf{X}_0 = [\ 10^{-4}\quad 6^\circ\quad 2^\circ\quad 0\quad 0\quad 0\quad 0\quad 0\ ]^{\mathrm{T}}$ for all conducted simulations. As to damping, it has been chosen equal to:

$$\begin{bmatrix} d_{1,1} & d_{1,2} & d_{1,3} \\ d_{2,1} & d_{2,2} & d_{2,3} \\ d_{3,1} & d_{3,2} & d_{3,3} \end{bmatrix} = \begin{bmatrix} 14.9950 & 1.2740 & 0.0264 \\ 1.2740 & 5.3513 & 0.0784 \\ 0.0264 & 0.0784 & 0.0059 \end{bmatrix}, \tag{29}$$

Table 1 – Simulation parameters used for conducting numerical simulations.

Parameter	Description	Value
b	Mid-chord [m]	0.125
a	Distance from semichord to elastic axis [–]	–0.5
c	Hinge line location mesuared from mid-chord [–]	0.5
ρ	Air density [kg/m^3]	1.078
m_W	Wing mass [kg]	1.5
m_T	Total mass [kg]	4.3723
ω_h	Plunge natural frequency [rad/s]	22.32
ω_α	Pitch natural frequency [rad/s]	20.08
ω_β	Control surface natural frequency [rad/s]	50.2761
x_α	Normalized distance between elastic axis and center of gravity of wing [–]	0.66
x_β	Normalized distance between hinge line and center of gravity of flap [–]	0.0028
r_α	Normalized rotational inertia term about elastic axis [–]	0.7303
r_β	Normalized rotational inertia term about hinge line [–]	0.0742
U^*	Linear case flutter onset velocity [m/s]	11.70

which corresponds, roughly, to 21 %, 24 %, and 0.1 % modal damping factors for the three vibration modes of the (linear) coupled system.

The viscoelastic material considered for the dampers is the Soundcoat® Dyad 606. It has been chosen since its maximum loss factor occurs, at ambient temperature, at a frequency that is close to the resonant frequencies of the aeroelastic system. The material temperature shift-factor is given by (Soovere and Drake, 1984):

$$\log_{10}\gamma(T) = A(1/T - 1/T_Z) + 2.303(2A/T_Z - B)\log_{10}(T/T_Z) + (B/T_Z - A/T_Z^2 - S_{AZ})(T - T_Z), \tag{30}$$

where temperature must be provided in Kelvin, and:

$$A = (D_B C_C - C_B D_C)/D_E; \quad B = (C_A D_C - D_A C_C)/D_E; \quad C_A = (1/T_L - 1/T_Z)^2; \quad C_B = (1/T_L - 1/T_Z);$$
$$C_C = S_{AL} - S_{AZ}; \quad D_A = (1/T_H - 1/T_Z)^2; \quad D_B = (1/T_H - 1/T_Z); \quad D_C = S_{AH} - S_{AZ}; \quad D_E = D_B C_A - C_B D_A;$$
$$\begin{bmatrix} T_Z & T_L & T_H & S_{AZ} & S_{AL} & S_{AH} \end{bmatrix} = \begin{bmatrix} 338 & 280 & 390 & 0.07 & 0.1142 & 0.03 \end{bmatrix}.$$

Following the identification procedure described from Eq. (10) to (14), and using data given by Soovere and Drake (1984) for the adopted viscoelastic material, it was possible to obtain $E_{0v} = 0.6066$ MPa, $E_{\infty v} = 1486.17$ MPa, $\tau_v = 0.221067$ μs, and $\alpha_v = 0.543794$, adopting $\nu = 0.5$. The summation involved in the discretization of the fractional derivative operator has been carried out considering $N_v = 100$.

Simulations have been run to investigate how the positioning of viscoelastic dampers influenced the system dynamic behavior. Scenarios have been considered such that viscoelastic damping was present at the plunge, pitch, and control surface degrees of freedom, each at a different time – i.e., first, $k_{hv} \neq 0$, and $k_{\alpha v} = k_{\beta v} = 0$; then $k_{\alpha v} \neq 0$, and $k_{hv} = k_{\beta v} = 0$; and finally $k_{\beta v} \neq 0$, and $k_{hv} = k_{\alpha v} = 0$.

To simplify the analysis, when viscoelastic damping has been considered, it was included as a percentile of the installed (linear) stiffness of the degree of freedom to which it was applied. For example, a percentile P of viscoelastic damping at pitch implies that:

$$G_{0v} k_{\alpha v} = P k_\alpha = P I_\alpha \omega_\alpha^2 = P(m_W b^2 r_\alpha^2)\omega_\alpha^2 \quad \Rightarrow \quad k_{\alpha v} = \tfrac{P}{G_{0v}} m_W b^2 r_\alpha^2 \omega_\alpha^2. \tag{31}$$

For the plunge and the control surface generalized coordinates, one would obtain $k_{hv} = \frac{P}{G_{0v}} m_W \omega_h^2$, and $k_{\beta v} = \frac{P}{G_{0v}} \cdot m_W b^2 r_\beta^2 \omega_\beta^2$, respectively. The results are presented in such a way that P_h, P_α and P_β refer to the percentiles related to the h, α, and β degrees of freedom, respectively. (Also, as explained before, when one of the percentiles differs from zero, the other two are null.)

Viscoelastic damping has been considered in amounts such that P_h ranged from 0 to 0.6%, P_α from 0 to 0.3%, and P_β from 0 to 50%. Physically, this corresponds to:

$$k_{hv} = 2.2174 \cdot 10^{-5}\ \mathrm{m}^{-1}; \quad k_{\alpha v} = 7.4779 \cdot 10^{-8}\ \mathrm{m}^3; \quad k_{\beta v} = 8.0655 \cdot 10^{-7}\ \mathrm{m}^3. \tag{32}$$

As a comparison, from Eq. (17), for a translational damper with $l_h = 10$ mm, $(d_2)_h = 0.5$ mm, and $(d_3)_h = 50$ mm, $k_{hv} = 2\ \mathrm{m}^{-1}$; whereas for a rotational damper with $R_{\mathrm{mean}} = 10$ mm, $d_2 = 0.5$ mm, and $d_3 = 50$ mm, $k_{\alpha v}$ or $k_{\beta v} = \pi \cdot 10^{-5}\ \mathrm{m}^3$. Thus, the values assumed for P_h, P_α, and P_β are more than realizable in a practical application, through a proper choice of the geometric parameters of the dampers.

As to the viscoelastic material temperature, it has been adopted equal to 25 °C and 35 °C, to show how this environmental condition impacts on the viscoelastic damped system response. Yet another simulation condition that has been considered is the one for which $c_v = 0$. This corresponds to the case where a viscoelastic damper has no energy dissipation, and its contribution consists of an addition to the system overall stiffness, only. The influence of a viscoelastic damper on the system behavior can then be attributed to an increase in its stiffness, or in its damping.

Figure 6 shows a plot of $F(\alpha)$ as given by Eq. (28), together with a comparison between the linearized and the nonlinear system responses (expressed as LCO amplitudes), without considering any viscoelastic damper yet. This shows that the flutter velocity for the linear system is approximately 11.70 m/s, which coincides with the nonlinear system bifurcation onset. Furthermore, this bifurcation is supercritical, as one has stated before.

Figures 7 to 9 show a collection of results expressed in the form of 3-D surfaces. In these it is possible to see the influence of the amount of viscoelastic damping, given in terms of P_h, P_α, and P_β, on the LCO amplitudes for the three degrees of freedom of the system. Figure 10 presents the LCO bifurcation onset speed U^* in terms of the percentiles P_h, P_α, and P_β. Figure 11 shows the LCO peak-to-peak amplitudes for the condition in which the airflow speed was set equal to 14 m/s. Finally, Fig. 12 contains time domain plots, phase diagrams, and the power spectrum density (PSD) for the three degrees of freedom, also for the condition of an airflow speed of 14 m/s.

An immediate inference from the presented results is related to the effectiveness of the viscoelastic damping in augmenting the LCO onset speed. When dampers are considered for the plunge and pitch degrees of freedom, a small amount of material is sufficient to raise the bifurcation speed from 11.70 m/s to more than 14 m/s, when temperature is 25°C (Fig. 10). In the case where the damper is installed in the control surface degree of freedom, even higher amounts of viscoelastic material are not sufficient to completely eliminate oscillations in all of the responses (although β peak-to-peak amplitudes are practically zero). This is credited to the small structural coupling that exists between the β and the

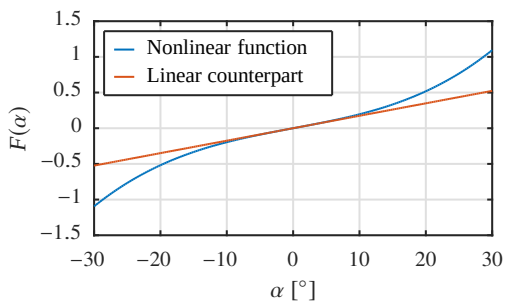

(a) Nonlinear stiffness function $F(\alpha)$

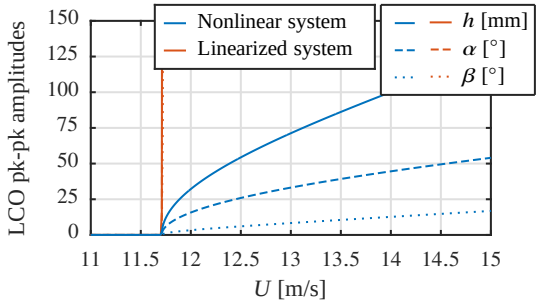

(b) Comparison between LCO amplitudes for the nonlinear system and its linearized counterpart

Figure 6 – Nonlinear characteristics of the simulated system.

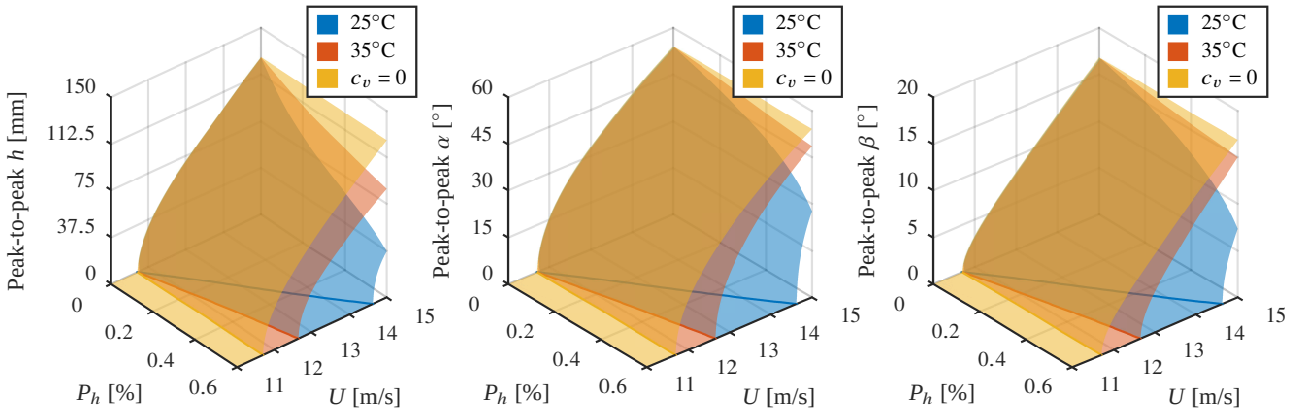

Figure 7 – Influence of viscoelastic damping in *h* on the LCO peak-to-peak amplitudes.

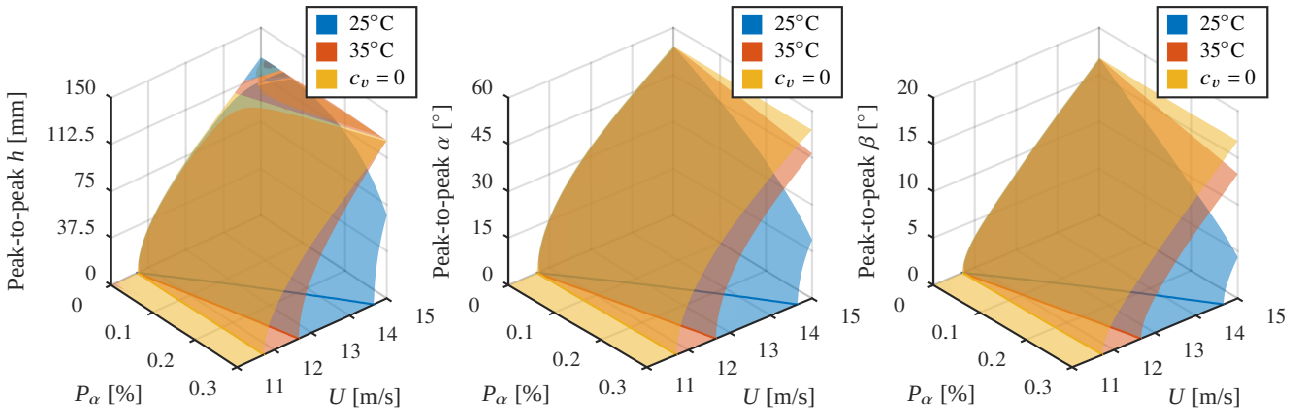

Figure 8 – Influence of viscoelastic damping in α on the LCO peak-to-peak amplitudes.

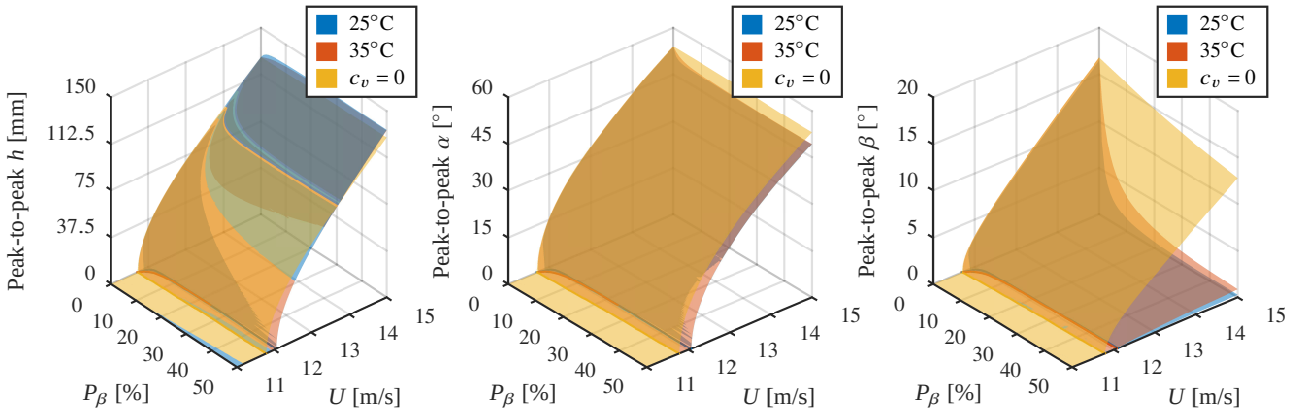

Figure 9 – Influence of viscoelastic damping in β on the LCO peak-to-peak amplitudes.

remaining degrees of freedom, which make it impossible for aeroelastic vibratory energy to flow from h and α to get dissipated in the viscoelastic damper.

Another important conclusion that can be drawn from the results is that the viscoelastic dampers reduce LCO ampli-

tudes and augment their velocity onset not by increasing the system stiffness, but through the addition of damping. This is made clear by comparing the curves associated to the condition $c_v = 0$ with the other ones, related to viscoelastic damping at temperatures of 25°C and 35°C in Figs. 10 and 11.

It is also possible to note that the dampers perform remarkably well at 25°C, and their performance suffers a major decrease when at 35°C. This happens because the viscoelastic material loss factor drastically reduces with an increase in temperature. This points in the direction that viscoelastic material selection must take into account the temperature at which it will operate. Then, damping levels can be predicted accurately, and the damper design can be successful. As results indicate, the performed simulations would clearly help mitigate issues of such nature.

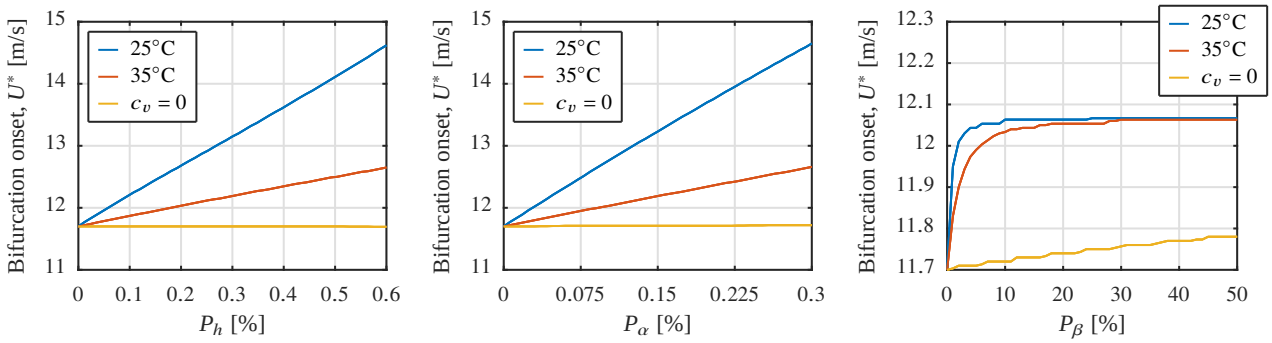

Figure 10 – Influence of viscoelastic damping on the bifurcation onset speed U^*.

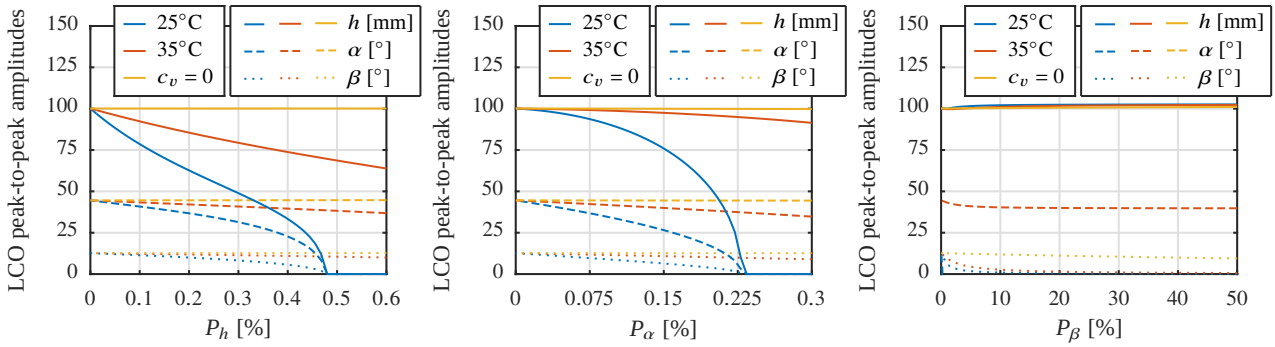

Figure 11 – Influence of viscoelastic damping on the LCO peak-to-peak amplitudes for $U = 14$ m/s.

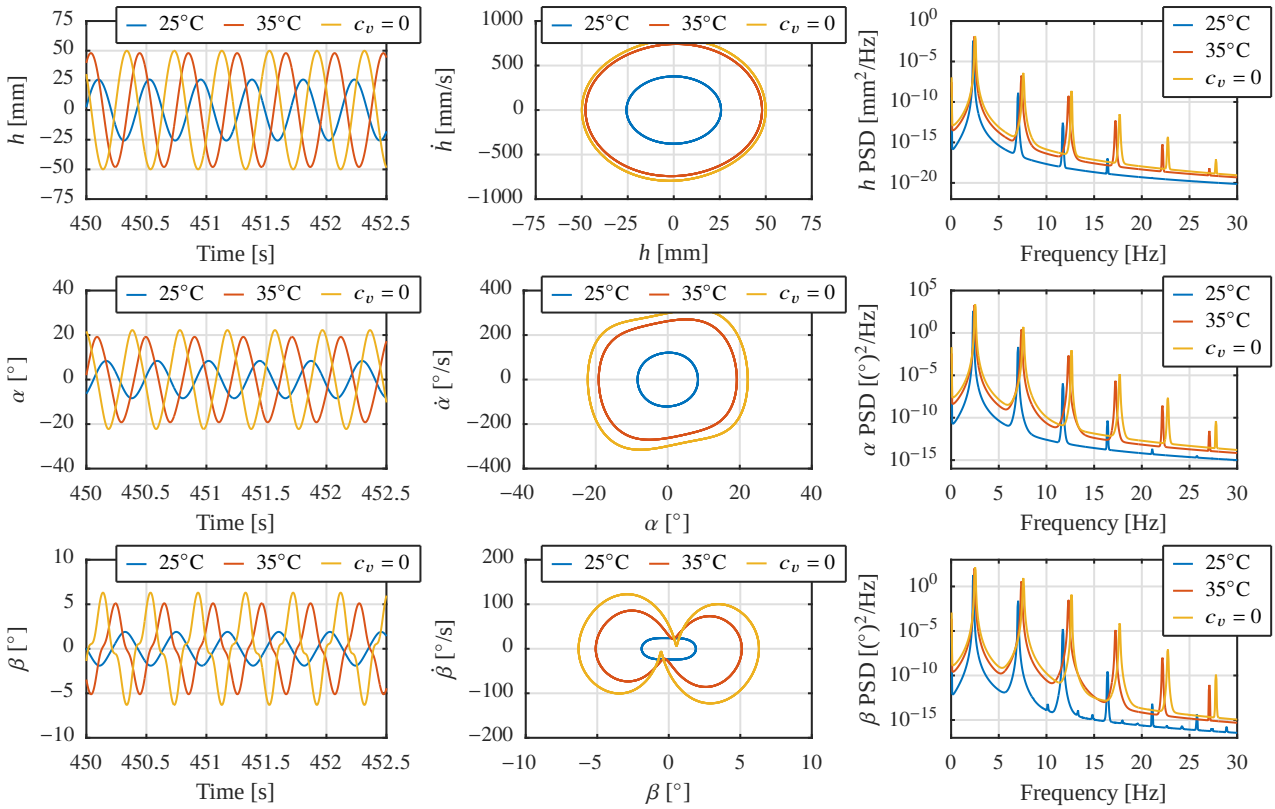

Figure 12 – Influence of viscoelastic damping seen in time domain plots, phase portraits, and power spectrum densities, for $U = 14$ m/s.

The time domain plots, Fig. 12, clearly show that steady state regime has been achieved, even when the system has small damping. The phase portraits also allow one to infer that LCO amplitude are reduced for the three degrees of freedom, when viscoelastic damping is added to the system. In the case of α and β, the nonlinear nature of the phase map even gets largely reduced for the case in which the viscoelastic material is at 25°C. The PSD plots show the nonlinear nature of the system in the frequency domain. Higher harmonics have much smaller energy densities in comparison with the one related to the fundamental frequency of the LCO. One more time, it can be seen that viscoelastic damping largely diminishes LCO amplitudes, and higher harmonics owned to nonlinear behavior.

CONCLUDING REMARKS

This paper has presented a methodology for the numerical simulation of a nonlinear typical section aeroelastic system with incorporated viscoelastic dampers. Viscoelastic modeling has been addressed with the use of Fractional Calculus, as a means to allow for efficient time integration of the resulting set of equations of motion.

The obtained results clearly show that viscoelastic damping can help mitigate issues that arise in aeroelastic systems. For the specific system considered in the paper, this is seen by the large increase the flutter speed (bifurcation onset) and also by the reduction of LCO amplitudes.

Numerical results have also shown that the incorporation of viscoelastic damping into the system must be performed carefully. This happens since temperature plays a major role in determining the material loss factor, for example. Also, the application of viscoelastic damping on the control surface degree of freedom did not produce results as those observed when viscoelastic dampers were applied to the plunge and pitch coordinates. In this sense, simulation tools, such as the one presented here, are of utmost valuable help.

ACKNOWLEDGMENTS

The authors acknowledge the National Council for Scientific and Technological Development (CNPq), and the Minas Gerais and São Paulo Research Foundations, FAPEMIG and FAPESP, respectively, for their continuing financial support of research activities.

REFERENCES

Bagley, R. L., and Torvik, P. J., 1986. On the fractional calculus model of viscoelastic behavior. Journal of Rheology, 30(1), 133-155.
Bisplinghoff, R. L., Ashley, H., and Halfman, R. L., 1996. Aeroelasticity. Dover Publications.
Chen, P. C., Sarhaddi, D., and Liu, D. D., 1998. Limit cycle oscillation studies of a fighter with external stores. AIAA paper, 1727.
Chung, K. W., He, Y. B., and Lee, B. H. K., 2009. Bifurcation analysis of a two-degree-of-freedom aeroelastic system with hysteresis structural nonlinearity by a perturbation-incremental method. Journal of Sound and Vibration, 320(1), 163-183.
Collar, A. R., 1946. The expanding domain of aeroelasticity. The Aeronautical Journal, 50(428), 613-636.
Cunha-Filho, A. G., de Lima, A. M. G., Donadon, M. V., and Leão, L. S., 2016. Flutter suppression of plates using passive constrained viscoelastic layers. Mechanical Systems and Signal Processing.
Diethelm, K., 2010. The analysis of fractional differential equations: An application-oriented exposition using differential operators of Caputo type. Springer.
Dowell, E., 2014. A Modern Course in Aeroelasticity (Vol. 217). Springer.
Dowell, E., Edwards, J., and Strganac, T., 2003. Nonlinear aeroelasticity. Journal of aircraft, 40(5), 857-874.
Galucio, A. C., Deü, J.-F., and Ohayon, R., 2004. Finite element formulation of viscoelastic sandwich beams using fractional derivative operators. Computational Mechanics, 33(4), 282-291.
Henshaw, M. D. C., Badcock, K. J., Vio, G. A., Allen, C. B., Chamberlain, J., Kaynes, I., ... and Jones, D., 2007. Non-linear aeroelastic prediction for aircraft applications. Progress in Aerospace Sciences, 43(4), 65-137.
Hodges, D. H. and Pierce, G. A., 2011. Introduction to structural dynamics and aeroelasticity (Vol. 15). Cambridge University Press.
Lacarbonara, W., and Cetraro, M., 2011. Flutter control of a lifting surface via visco-hysteretic vibration absorbers. International Journal Aeronautical and Space Sciences, 12(4), 331-345.
Lakes, R. S., 2009. Viscoelastic Materials. Cambridge University Press.
Martins, P. C., Guimarães, T. A., Pereira, D. D. A., Marques, F. D., and Rade, D. A., 2017. Numerical and experimental investigation of aeroviscoelastic systems. Mechanical Systems and Signal Processing, 85, 680-697.
Nashif, A. D., Jones, D. I., and Henderson, J. P., 1985. Vibration damping. Wiley-Interscience.
Nayfeh, A. H., and Balachandran, B., 2008. Applied nonlinear dynamics: analytical, computational and experimental methods. John Wiley & Sons.
O'Neil, T., and Strganac, T. W., 1998. Aeroelastic response of a rigid wing supported by nonlinear spring. J. Aircr, 35(4), 616-622.
Rao, M. D., 2003. Recent applications of viscoelastic damping for noise control in automobiles and commercial airplanes. Journal of Sound and Vibration, 262(3), 457-474.
Sheta, E. F., Harrand, V. J., Thompson, D. E., and Strganac, T. W., 2002. Computational and experimental investigation of limit cycle oscillations of nonlinear aeroelastic systems. Journal of Aircraft, 39(1), 133-141.
Soovere, J., and Drake, M. L., 1984. Aerospace structures technology damping design guide, Vol III: Damping material data. AFWAL Technical Report 84-3089.
Theodorsen, T., 1935. General theory of aerodynamic instability and the mechanism of flutter, tech. rep., NACA Report 496.
Vasconcellos, R. M., Abdelkefi, A., Hajj, M. R., Almeida, D. P., and Marques, F. D., 2016. Airfoil control surface discontinuous nonlinearity experimental assessment and numerical model validation, J. Vib. Control., 22(6), 1633-1644.
Vasconcellos, R. M., Abdelkefi, A., Marques, F. D., and Hajj, M. R., 2012. Representation and analysis of control surface freeplay nonlinearity. Journal of Fluids and Structures, 31, 79-91.

RESPONSIBILITY NOTICE

The authors are the only responsible for the printed material included in this paper.